Title
The Mainshock-aftershock Seismic Risk Analysis of a Steel Frame Using Energy-based Damage Index

Author
YAO, Kunliang

Publication Date
2019

Peer reviewed|Thesis/dissertation

UNIVERSITY OF CALIFORNIA

Los Angeles

The Mainshock-aftershock Seismic Risk Analysis of a Steel Frame Using Energy-based Damage Index

A thesis submitted in partial satisfaction

of the requirements for the degree Master of Science

in Civil Engineering

by

Kunliang Yao

2019

ABSTRACT OF THE THESIS

The Mainshock-aftershock Seismic Risk Analysis of A Steel Frame

Using Energy-based Damage Index

by

Kunliang Yao

Master of Science in Civil Engineering

University of California, Los Angeles, 2019

Professor Henry V. Burton, Chair

Structures are generally under the risk of earthquake events, especially in regions with high seismicity. However, rather than occur individually, the seismic events are tend to happen in sequence of the mainshock and the multiple aftershocks, which would cause additional damage to the damaged buildings in post-mainshock environment and increase the probability of collapse. This study mainly focuses on characterizing the seismic risk of a 4-story steel frame under mainshock-aftershock earthquake sequences. The damage of the structure are captured using the maximum story drift ratio and the energy-based damage indices, of which the performances are evaluated and compared in prior. The result shows that the energy-based damage index has higher ability to capture the potential structural damage and tend to display higher rate of collapse in the lifetime of buildings.

The thesis of Kunliang Yao is approved.

John Wright Wallace

Yousef Bozorgnia

Henry V. Burton, Committee Chair

University of California, Los Angeles

2019

Table of Contents

List of Figures

List of Tables

Chapter 1 Introduction

1.1 Motivation

When a mainshock of earthquake occurs, it will be generally followed by a sequence of ground motions with relatively lower intensities. These small following seismic events are called "aftershocks". Despite aftershocks usually having smaller intensities than their preceding mainshocks, their higher rate of occurrence will leave less time for repair or retrofit of the damaged buildings. Furthermore, if a building is considerably damaged in the mainshock event, the aftershocks will be more likely to cause further damage to the building, leading to the extra financial loss and fatalities. The downtime for building repairing after the seismic events would therefore be elongated with the occurrence of aftershocks. Hence, it is necessary to take the mainshock-aftershock (MS-AS) sequence effect into consideration when performing seismic risk analysis.

The performance-based earthquake engineering (PBEE) [1] proposed by the Pacific Earthquake Engineering Research Center (PEER) has become a standard practice in the seismic design of new structures or the evaluation of seismic performance of existing buildings. It provides engineers and researchers with a probabilistic approach, for seismic risk evaluation. This allows for the incorporation of different sources of uncertainty into the seismic risk assessment of structures.

As part of the probabilistic framework of PBEE, the Probabilistic Seismic Hazard Analysis (PSHA) is used to quantify the variability of different sources to seismic hazard. The annual rate of exceedance of a certain intensity measure (IM) of a ground motion for a structure in a specific location is an important feature. In traditional PSHA, which is typically developed with the truncated exponential magnitude model or a characteristic magnitude model, the annual rate of

occurrence of mainshock with a given IM level is treated as a constant, time-invariant value. However, when evaluating the aftershock events, the rate of occurrence would be time-variant. The aftershock rate will be decaying with the elapsed time since the mainshock event. In the meantime, the magnitude of the aftershocks is usually dependent on the magnitude of antecedent mainshock event. To capture these natures of the aftershock, Yeo and Cornell [2] proposed the aftershock PSHA (APSHA) by introducing a rate accounting for the decaying rate of aftershock occurrence with the elapsed time since the mainshock's occurrence.

Damage measure (DM) is also a significant component of seismic risk analysis in the PBEE' framework. It is used as a measure of the structural damage in an earthquake even and is calculated from the engineering demand parameter (EDP) which is typically directly obtained from the dynamic structural responses and is utilized in defining the damage state (DS) of the structure. Many indices have been considered as the performance indicators in evaluating the seismic risk and researchers are more interested in those with higher correlation with structure damage. Traditionally, some of the EDPs can be directly treated as DMs. Typically, the story drift ratio and the peak floor acceleration (PFA) are widely used by researchers. However, the SDR and the PFA sometimes cannot identify the real structural damages, especially when the seismic events are smaller in intensity and longer in time duration. In recent years, many researchers have put forward a new type of damage indices to be used as the DMs that is calculated based on the hysteretic response of structure elements [3][4][5][6]. This type of energy-based damage indices uses the hysteretic energy of structural elements, sometimes combining with other features (e.g., the maximum deformation), to describe the damage of structures.

These energy-based damage indices are cumulative, in contrast to the traditional non-cumulative damage indicators. However, few studies are devoted to the evaluation of the

performance of those indices in seismic risk analysis. Estekanchi [7] compared the correlation between the Park-Ang damage index D_{PA} and other types of damage index using the dynamic responses of a steel frame based on the endurance time analysis. Tesfamarim and Goda [8] compared the Mehanny-Deierlein damage index D_{MD} with story drift ratio based on the performance of a 15-story concrete building with shear walls at the centroid core under a series of MS-AS ground motions. A systematic evaluation of different energy-based damage indices would help researchers make better decisions in selecting a proper damage indicator in various situations.

1.2 Objectives

The main objective of this study is to compare the performance of a set of energy-based damage indices and a group of more traditional EDPs for seismic risk analysis under sequential MS-AS ground motions. A numerical model of a 4-story 2-bay steel frame is used as a benchmark. Several energy-based damage indices are used as the damage indicators. Incremental dynamic analysis (IDA) is adopted as the main analysis approach.

The output data of mainshock of some certain intensity measure levels are used to compare the effectiveness of different energy-based indices with the story drift, which is a widely-used damage indicator. The comparison is based on the statistical features of the index and to which extent the index can reflect the real damage in the structure.

The outputs of MS-AS risk analysis are used to evaluate the additional contribution of the aftershock to seismic risk when different indices are used as the damage indicator.

1.3 Organization

This study seeks to evaluate the collapse risk of a steel frame under different MS-AS ground motion sequences when different indices are used as the damage indicator. The whole body of the thesis consists of 4 chapters. Chapter 1 discusses the significance of the systematic evaluation of energy-based damage indices that are used in the MS-AS seismic risk analysis to describe the damage of structure.

Chapter 2 describes the steps of building the numerical model of the steel moment frame structure and the characteristics of the set of MS-AS ground motions used for the MS-AS response history analyses.

Chapter 3 introduces the definition of 3 different energy-based damage indices that would be evaluated and applied to analyzing the seismic risk of the steel frame in the following chapters. The approach of calculating the damage indices using the output data from incremental dynamic analysis is also discussed in this chapter.

Chapter 4 discusses the steps of comparing the effectiveness of energy-based damage indices and the SDR as the measure of structural damage by analyzing the statistical features of the calculated results of the index and whether the index can reflect the real damage in the structure based on the output results of mainshock dynamic analysis.

Chapter 5 is mainly focused on the MS-AS seismic risk analysis using different damage indices. Markov process will be applied in calculating the risk of transition from a certain pre-mainshock damage level to the aftershock damage state.

Chapter 2 The Numerical Model of the Steel Frame and Ground Motions Selection

This chapter consists of three parts. The first part of this chapter will discuss the steps taken for building the numerical model of a 4-story steel moment frame used in the dynamic analysis. The second part of this chapter will focus on the selection of the MS-AS ground motion records that would be used as the input ground motion in the response history analysis. The output data of the numerical model after it is subjected to the selected set of earthquake ground motions will form the inputs that will be used to evaluate the effectiveness of damage indices in Chapter 3 and to compute the MS-AS seismic risk in Chapter 4. In the last part of the current chapter, the method of calculating the energy-based damage indices using the output data from IDA and using the damage indices to describe the element-level (or local) damage and structure-level (or global) damage will be discussed.

2.1 Numerical Model

A 4-story code-compliant steel moment-resisting frame is used in this study. The numerical model of this steel frame is adopted from the model developed by Lignos et al [9] and is located in the Los Angeles area. The prototype building is designed for the horizontal and vertical loads according to the provisions of 2003 IBC [10] and AISC 341-05 [11]. The steel frame is a special moment frame (SMF) with reduced beam sections designed according to FEMA 350 [12]. The story height is 15 feet (4.6 m) for the base story and 12 feet (3.7 m) for other stories. The span length is 30 feet (9.1 m) for each bay.

A 2-D nonlinear model of the steel frame is built in OpenSees [13], one of the most widely-used platform for numerical simulation of structures. A set of MS-AS ground motion sequences will be applied to the numerical model in OpenSees. Figure 2.1 shows a schematic layout of the numerical model. The entire numerical model consists of the lateral system and the gravity system. In the lateral system, the beams and columns are modeled using elastic elements with uniaxial moment-rotation hinges at the ends to describe the concentrated inelasticity. The gravity system is modeled using a leaning column rigidly linked to the lateral system to represent the $P-\Delta$ effect. The nodal masses are concentrated at each level of the leaning column. The fundamental period (T_1) of this model is 1.42 sec, which is obtained from the eigen-value analysis.

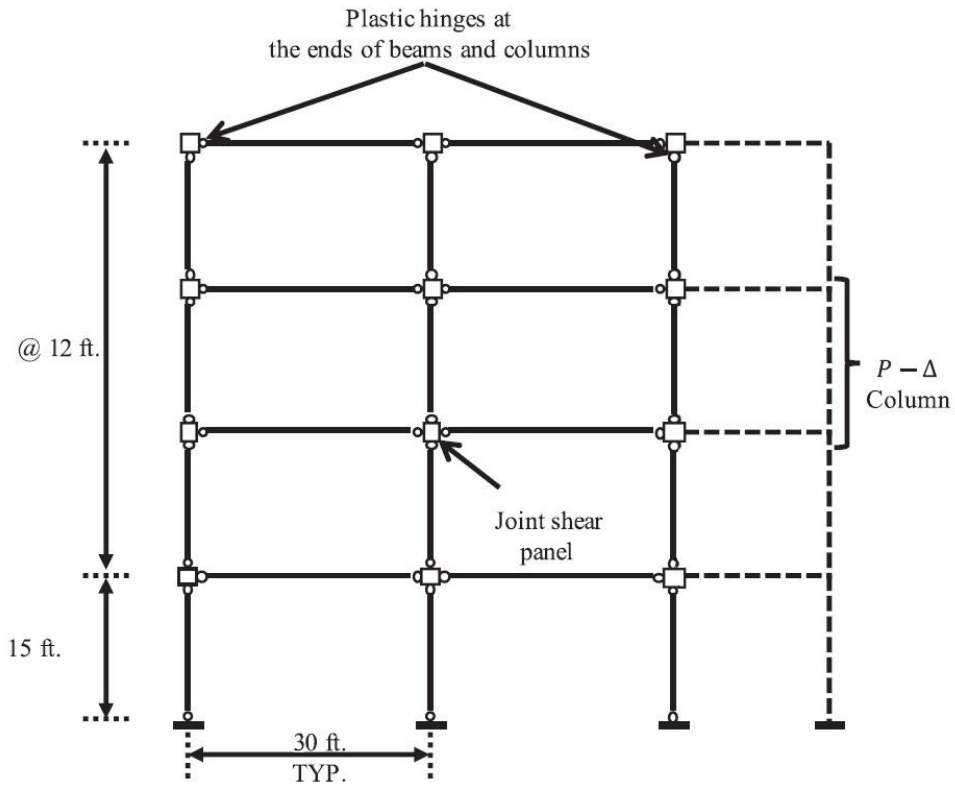

Figure 2.1 Elevation Layout of Numerical Model

The nonlinear behavior of the moment-rotation hinges is modeled using the modified Ibarra-Medina-Krawinkler model with bilinear hysteretic response [14], which is able to capture the effect of strength and stiffness deterioration when the structure experiences the repetitive loading and unloading cycles in earthquake. The input values of the hinge models are obtained from the experimental data presented by Lignos et al [9].

2.2 Ground Motion Sequences Selection

The evaluation of damage indices and the seismic risk analysis require a series of nonlinear dynamic analysis with the numerical model mentioned previously subjected to a suite of MS-AS ground motion sequences. In the previous studies, four approaches are used to generate the MS-AS sequences to conduct the seismic structural analysis: (1) the mainshock-mainshock (MS-MS) approach; (2) the targeted mainshock-mainshock (TG-MS-MS) approach; (3) the same-sequence MS-AS (SS-MS-AS) approach; (4) the different-sequence mainshock-mainshock (DS-MS-MS) approach [15]. It is shown that the artificial ground motion sequences would lead to biased results comparing to the as-record ground motion sequences. Goda [16] used the mainshock-mainshock records and the same-sequence MS-AS records to evaluate the collapse performance of a 2-story wood frame and it is shown that the MS-MS records will give higher likelihood of collapse. Ruiz-García [17] drew the same conclusion based on his study of two steel frames with different height. Abrahamson et al. [18] found significant differences between the spectral values of mainshock and aftershock records at different ranges of structural period. The study conducted by Boore et al. [19] showed that the DS-MS-AS approach is less likely to preserve the correlation between mainshocks and aftershocks. Hence, the SS-MS-AS approach is considered best for the response

history analysis because of its ideal performance in capturing the natural relationship between mainshock and aftershock ground motions.

For the reasons given above, a set of SS-MS-AS ground motion sequences that are recorded from the past earthquakes are selected from the NGA-West2 database, one of the largest ground motion database compiled by the Pacific Earthquake Engineering Research Center (PEER) [20]. The ground motion set includes 32 MS-AS records selected from 11 earthquake events. A magnitude-dependent time window and a distance threshold of 40 km measured in terms of the centroidal Joyner-Boore distance [19] is used to identify the aftershock ground motions following a mainshock event. The earthquake events from which the MS-AS sequence records are selected have magnitudes ranging from 5.80 to 7.62 for mainshocks and from 5.01 to 6.20 for aftershocks. The Joyner-Boore distances (R_{jb}) range from 0 to 43.6 km for mainshocks and are within the 5.56 to 85.42 km window for aftershocks. Table 2-1 summarizes the properties of each pair of MS-AS ground motion sequence record. The response spectra of the suite of mainshock and aftershock ground motions measured in terms of peak spectral acceleration (PSA) are shown in Figure 2.2 with the median spectra curves highlighted.

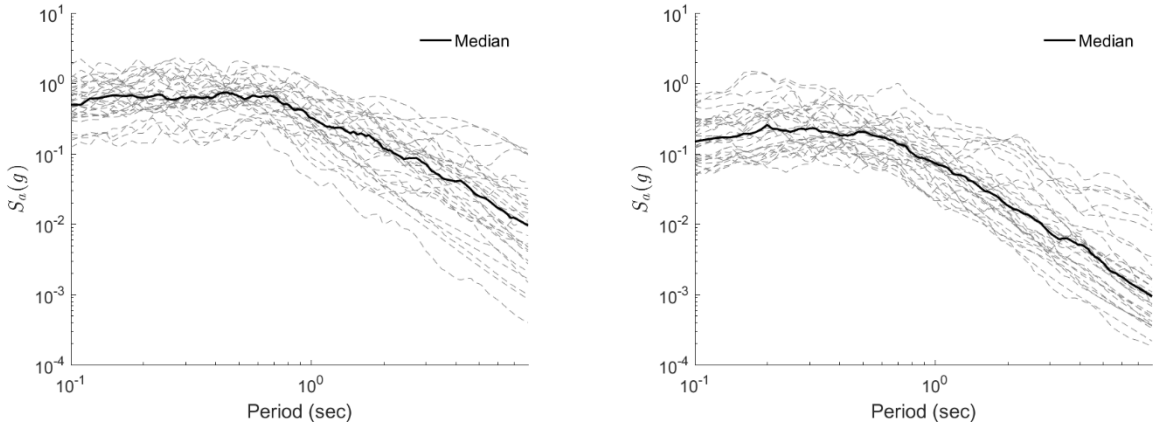

(a) (b)

Figure 2.2 Response Spectra of (a) Mainshock; (b) Aftershock Ground Motions

Table 2-1 Information of the MS-AS Ground Motion Sequences

Sequence ID	Event name	Mainshock ground motion			Aftershock ground motion		
		M_w	$R_{jb}(km)$	$V_{s30}(m/s^2)$	M_w	$R_{jb}(km)$	$V_{s30}(m/s^2)$
1	Imperial Valley-06	6.53	7.29	242.05	5.01	11.17	231.23
2	Imperial Valley-06	6.53	22.03	242.05	5.01	23.76	237.33
3	Northridge-01	6.69	12.39	545.66	5.2	20.08	508.08
4	Northridge-01	6.69	9.44	355.81	5.93	22.23	450.28
5	Northridge-01	6.69	11.39	325.6	5.93	25.63	508.08
6	Northridge-01	6.69	20.11	450.28	5.28	18.29	379
7	Northridge-01	6.69	0	380.06	5.28	9.15	440.54
8	Livermore-01	5.8	15.19	377.51	5.42	27.76	517.06
9	Coalinga-01	6.36	23.78	274.73	5.09	24.23	467.03
10	Coalinga-01	6.36	7.69	257.38	5.18	5.56	478.63
11	Coalinga-01	6.36	7.69	257.38	5.18	5.56	478.63
12	Landers	7.28	2.19	1369	6.46	34.98	296.97
13	Mammoth Lakes-01	6.06	1.1	382.12	5.69	14.28	537.16
14	Mammoth Lakes-01	6.06	12.56	537.16	5.91	10.31	537.16
15	Chalfant Valley-02	6.19	21.55	370.94	5.44	23.99	303.47
16	Whittier Narrows-01	5.99	32.56	297.71	5.27	34.36	318.16
17	Whittier Narrows-01	5.99	10.31	267.13	5.27	22.21	316.02
18	Whittier Narrows-01	5.99	20.37	320.57	5.27	23.98	297.07
19	Whittier Narrows-01	5.99	14.95	271.9	5.27	25.36	550.11
20	Whittier Narrows-01	5.99	14.68	371.07	5.27	22.93	270.96
21	Umbria Marche, Italy	6	18.86	401.34	5.5	35.83	492
22	Umbria Marche, Italy	6	8.29	428	5.5	16.84	376.6
23	Darfield, New Zealand	7	43.6	638.39	6.2	85.42	638.39
24	Darfield, New Zealand	7	7.29	326.01	6.2	17.86	255
25	Darfield, New Zealand	7	24.36	422	6.2	57.72	481.62
26	Darfield, New Zealand	7	30.53	255	6.2	66.53	561.03
27	Darfield, New Zealand	7	5.07	263.2	6.2	9.05	263.2
28	Chi-Chi, Taiwan	7.62	33.19	347.63	6.2	36.38	378.75
29	Chi-Chi, Taiwan	7.62	3.12	542.61	6.2	27.88	277.5
30	Chi-Chi, Taiwan	7.62	10.96	544.74	6.2	23.44	542.61
31	Chi-Chi, Taiwan	7.62	12.6	573.04	6.2	33.86	573.04
32	Chi-Chi, Taiwan	7.62	16.04	233.14	6.2	40.79	492.26

Chapter 3 Energy-based Damage Indices

In the majority of past studies, the damage state of structures under a seismic cyclic loading has been described using the maximum story drift ratio, the maximum roof drift ratio or the peak floor acceleration. These EDPs usually work well if the buildings are subjected to ground motions that are relatively strong in intensity. But a structure might also experience relatively high degrees of damage under earthquakes with lower magnitude but longer time duration, where the traditional methods sometimes fail to capture the real structural damages. As such, a number of studies have tried to involve the energy dissipated during the inelastic cyclic loading in defining the damage level of structures. This chapter introduces 3 different indices describing the damage level of structures under the seismic loading based on the absorbed energy. These damage indices are evaluated based on the concepts of efficiency and sufficiency and compared with the maximum story drift ratio as the traditional damage measure in Chapter 4. in Chapter 5, these damage indices are used as the damage measures (DMs) in the MS-AS seismic risk analysis.

3.1 The Park-Ang Damage index D_{PA}

In 1985, Park and Ang [4] introduced a seismic structural damage index for reinforced concrete members defined as a linear combination of two terms: the maximum deformation and the hysteretic energy, which is expressed in form of Equation 3.1.

$$D_{PA} = \frac{\delta_M}{\delta_u} + \frac{\beta}{Q_y \delta_u} \int dE \tag{3.1}$$

The first term is the ratio of the maximum deformation response δ_M in dynamic analysis and the ultimate deformation capacity δ_u obtained from the static analysis. The second term is a factored ratio of the total dissipated energy and the energy capacity. Q_y is the calculated yield strength and β is a coefficient for cyclic loading effect which is selected based on the experimental data.

The Park-Ang damage index was initially calibrated against the observation of seismic damage of reinforced concrete members. For the most significant coefficient β, Park and Ang proposed an empirical equation for concrete members based on the shear span ratio, the longitudinal reinforcement ratio and the axial stress [21]. A few studies have attempted to extend the coefficient's scope and make it applicable to steel frame buildings. Consenza et al. [22] recommended that the coefficient β for steel members should be taken as 0.15.

The Park-Ang damage index is among the most popular indices because of its conceptual simplicity. However, it also presents several deficiencies: 1) the format of linear combination of deformation and energy parts in spite of their underlying nonlinearity and interdependence, 2) the lack of considering the loading sequence effect and 3) the incapability to converge to zero even if the structure remains in elastic state.

Besides the incapability to give zero value when the structure remains elastic, Bozorgnia and Bertero [23] also argued that the Park-Ang damage index D_{PA} has the drawback that the index would fail to give the correct damage value for structures in monotonic loading. To overcome these two drawbacks, Bozorgnia and Bertero proposed an improved damage index which has better performance at extreme cases. The improved damage index shows a good correlation with D_{PA} in a reliable intermediate range.

It is worthwhile noting that the Park-Ang damage index D_{PA} is a local-level damage index, which means it only represents the damage condition of a single component in the structure. The global damage index can be computed by assigning a relative weight to the local damage indices of the structural components. Park and Ang proposed a total damage index D_T as

$$D_T = \frac{\Sigma E_i D_i}{\Sigma E_i} \tag{3.2}$$

Where D_i is the local damage index for component i and E_i is the corresponding dissipated energy for component i which is also incorporated in the damage index calculation.

3.2 The Kratzig Damage Index D_K

To account for the effect of cyclic loading sequences, Kratzig et al. [5] has proposed an energy-based index D_K that is based on the concepts of primary half cycles (PHCs) and follower half cycles (FHCs) for reinforced concrete members. The index is expressed in the form of Equations 3.3-3.5.

$$D_K^+ = \frac{\Sigma E_{PHC,i}^+ + \Sigma E_{FHC,i}^+}{E_f^+ + \Sigma E_{FHC,i}^+} \tag{3.3}$$

$$D_K^- = \frac{\Sigma E_{PHC,i}^- + \Sigma E_{FHC,i}^-}{E_f^- + \Sigma E_{FHC,i}^-} \tag{3.4}$$

$$D_K = D_K^+ + D_K^- - D_K^+ D_K^- \tag{3.5}$$

Where D_K^+ and D_K^- are the Kratzig damage index for the positive and negative parts of the structural response, respectively. $E_{PHC,i}^+$ and $E_{PHC,i}^-$ account for the energy dissipated in the ith

primary half cycle (PHC) of response, while $E^{+}_{FHC,i}$ and $E^{-}_{FHC,i}$ represent the dissipated energy of the ith follower half cycle (FHC). E_f^{+} and E_f^{-} are the energy absorbed by the component from the undamaged state to failure, which is obtained from a monotonic test. For a symmetric section, E_f^{+} and E_f^{-} can be assumed to be equal.

An essential distinction of the Kratzig damage index from the other damage indices is the introduction of the primary half cycles (PHCs) and the follower half cycles (FHCs). As it is shown in Figure 3.1, the PHC is established when the maximum deformation of a certain half cycle of response exceeds its previous half cycle, otherwise, the FHCs would be following consecutively.

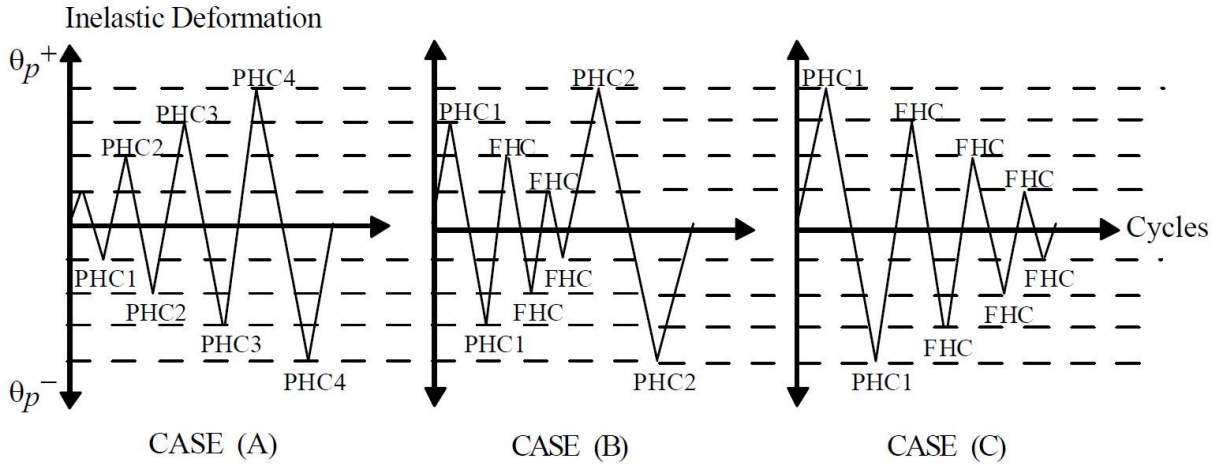

Figure 3.1 Definition of PHC and FHC under Different Loading Sequences

Compared to the traditional damage measures and the Park-Ang damage index D_{PA}, the Kratzig damage index D_K could be more computationally involved. However, the strengths are obvious: 1) Treating the positive and negative parts of the cyclic response infividually is useful to handle elements with an unsymmetrical section, 2) PHCs and FHCs help the damage index capture the

damage evolution paths more accurately and 3) the way PHC and FHC are arranged in the index equations ensures that the PHCs have strong influence on the abrupt damage increments while the FHCs contribute more to the long-term damage.

3.3 The Mehanny-Deierlein Damage Index D_{MD}

By introducing calibration parameters for the PHC and FHC values, Mehanny and Deierlein [6] extended the Kratzig damage index and associated it with different type of components including reinforced concrete columns, steel beams and composite joint panels, et al. The damage index is expressed in form of Equations 3.6 to 3.8.

$$D_{MD}^{+} = \frac{\left(\Sigma E_{PHC,i}^{+}\right)^{\alpha} + \left(\Sigma E_{FHC,i}^{+}\right)^{\beta}}{\left(E_{f}^{+}\right)^{\alpha} + \left(\Sigma E_{FHC,i}^{+}\right)^{\beta}} \tag{3.6}$$

$$D_{MD}^{+} = \frac{\left(\Sigma E_{PHC,i}^{-}\right)^{\alpha} + \left(\Sigma E_{FHC,i}^{-}\right)^{\beta}}{\left(E_{f}^{-}\right)^{\alpha} + \left(\Sigma E_{FHC,i}^{-}\right)^{\beta}} \tag{3.7}$$

$$D_{MD} = \sqrt[\gamma]{(D_{MD}^{+})^{\gamma} + (D_{MD}^{-})^{\gamma}} \tag{3.8}$$

Where α, β and γ are the calibration parameters determined from the physical damage observed in experimental tests. For steel components, Mehanny and Deierlein have suggested the values of $\alpha = 1.0$, $\beta = 0.95$ and $\gamma = 6.0$.

Mehanny and Deierlein also recommended that the available plastic energy capacity for steel components should be expressed as Equation 3.9, which is the area of the shaded part in Figure 3.2.

$$E_f = 1.15 M_p \theta_p \tag{3.9}$$

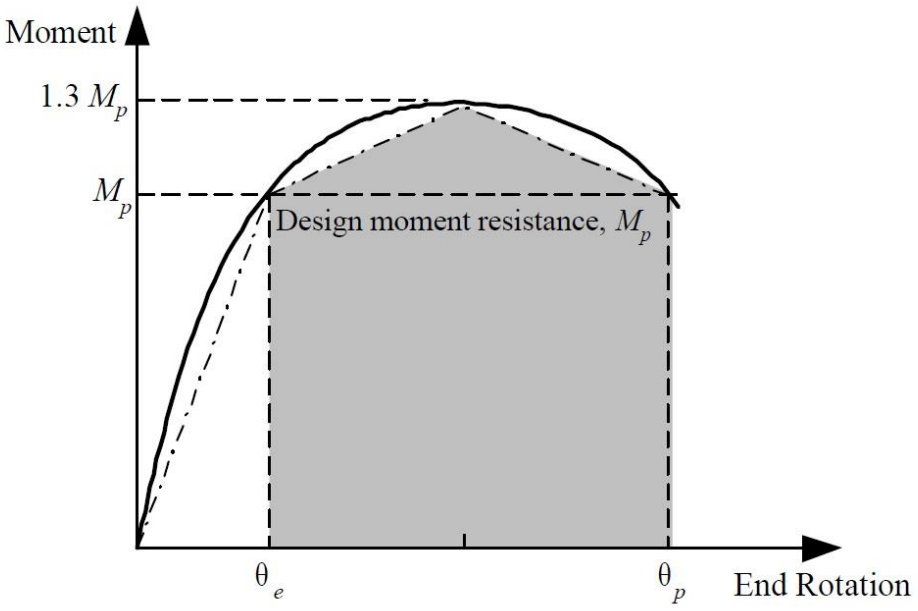

Figure 3.2 Mehanny & Deierlein's Definition of Plastic Energy Capacity

Where the plastic rotational capacity θ_p is the rotation available beyond the elastic rotation capacity θ_y, and right before the moment dropping below the yielding moment M_p. This suggestion is based on the assumption that the maximum moment capacity is approximately $1.3M_p$ observed from experimental data and the point of maximum moment is roughly corresponding to half the plastic rotational capacity concluded by Kemp et al. [24]

However, this equation for energy capacity E_f is found to be too conservative based on the calculation results in the following chapters. In this study, the plastic energy capacity for steel members used in the Kraztig damage index D_K and the Mehanny-Deierlein damage index D_{MD} is taken as the absorbed energy in terms of the hinge rotation from the yielding point of the component to the point prior to the moment reaching the residual moment in a monotonic loading test.

Chapter 4 Comparison and Evaluation of the Energy-based Damage Indices

In this chapter, IDA is applied to the numerical model of a steel moment frame using the selected suite of ground motions discussed in Chapter 2. The energy-based damage indices, whose calculation methods are given in Chapter 3, are computed from the outputs of IDA under only the mainshock ground motions. The maximum story drift ratios ($MaxSDR$s) are also recorded, as the traditional widely-used damage measure, to compare with the energy-based damage indices. The comparison is based on the concept of efficiency and sufficiency proposed by Luco and Cornell [25] initially. The correlation between the time duration of ground motions and damage measure caused under the corresponding ground motion are also considered in the evaluation.

4.1 Method of Incremental Dynamic Analysis (IDA)

In this chapter, IDA is performed under the set of 32 mainshock ground motion records described in Chapter3. In order to simulate the response of the steel moment frame building under a broad range of ground motion intensities, the ground motions are incrementally scaled to 20%, 40%, 60%, 80% and 100% of the Maximum Considered Earthquake (MCE) level. Hence, the dynamic analysis is carried out with 160 scaled ground motions in total.

to calculate the various damage measures considered in this study, different types of structural responses are recorded, including the story drift ratio histories at all 4 stories, the rotation and moment responses of all the plastic hinges and the displacement, velocity and acceleration of each degree of freedom of the structural nodes.

4.2 Damage Measure Response from IDA

Based on the recorded data mentioned above, the structural damage measures corresponding to each scaled ground motion record, including the maximum story drift ratio ($MaxSDR$) and the 3 kinds of energy-based damage indices discussed in Chapter 3 are calculated. Statistical evaluation of those damage measures is conducted based on these outputs.

Figure 4.1 illustrates the history of the $MaxSDR$ and the Mehanny-Deierlein damage index D_{MD} under the mainshock ground motion of Landers (sequence No.12 in Table 2-1) at 100% MCE of intensity level. It is worthy to note that the maximum SDR will occur in different story at different time point. The time history of the $MaxSDR$ is capturing the drift of the story where the maximum SDR occurs in the structure. Figure 4.2 shows the $MaxSDR$ at each story level. The $MaxSDR$ profile shows that the largest values tend to occur at the 1st story in most cases. Figure 4.3 shows the relationships between the damage measures and the spectral acceleration at the structural fundamental period $T_1 = 1.42\ sec$, for all the MS records. The $S_a(T_1) - DM$ plots in Figure 4.3 display that the $MaxSDR$ has the highest correlation with $S_a(T_1)$, while the energy-based damage measures are presenting a bilinear relationship with the spectral acceleration. This is due to the combined effect of the maximum deformation and the hysteretic energy on the energy-based indices. For D_K and D_{MD}, the calculation of the indices is highly dependent on the absorbed energy of structural members. When the intensity of ground motion is small, the structure mostly remains elastic and does not absorb much earthquake energy, leading to a small calculated damage index. As the intensity level increases, the structure begins to absorb more energy and therefore starts to develop structural damage measurable in terms of D_K and D_{MD}. For D_{PA}, the maximum deformation and hysteretic energy both contribute significantly to the calculation of D_{PA} and as

such, the jump discontinuity in the its observed values in Figure 4.3b is not as notable as D_K and D_{MD}. Usually the structural responses at larger intensities are more of importance. Hence, if only data points with $Sa(T_1) > 0.2g$ are considered, all the damage measures would exhibit a linear correlation with the spectral acceleration. These relationships are also used in the quantitative measure of efficiency and sufficiency [25], which will be discussed later in this chapter.

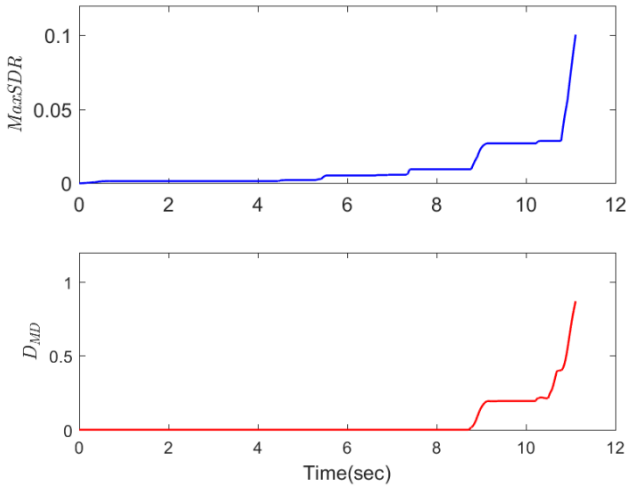

Figure 4.1 Time History of $MaxSDR$ and D_{MD} under Landers at 100% of MCE Level

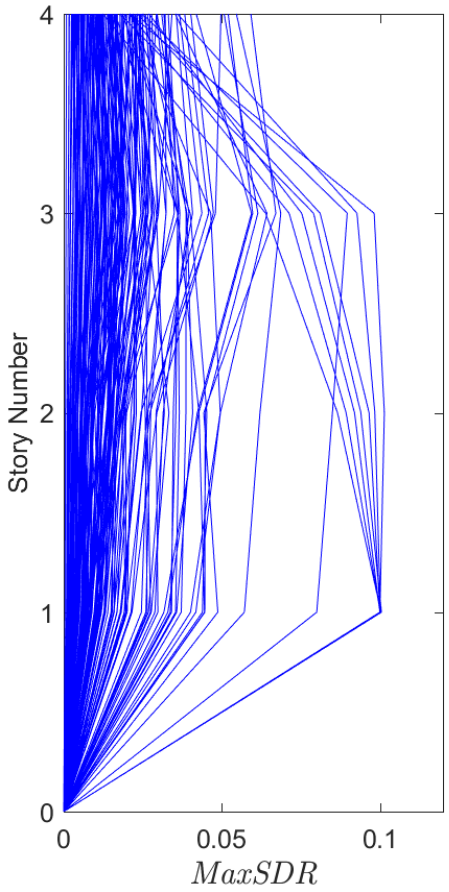

Figure 4.2 $MaxSDR$ along the building height

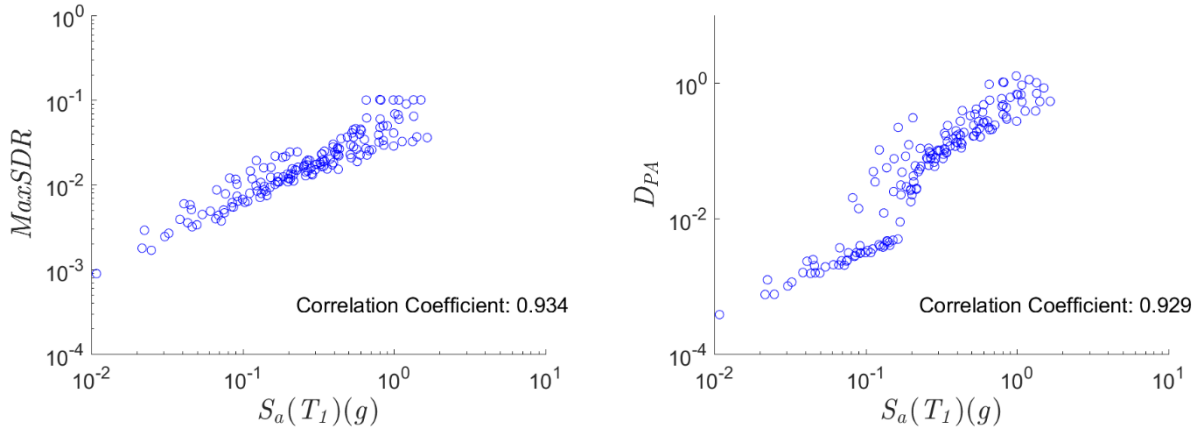

(a) (b)

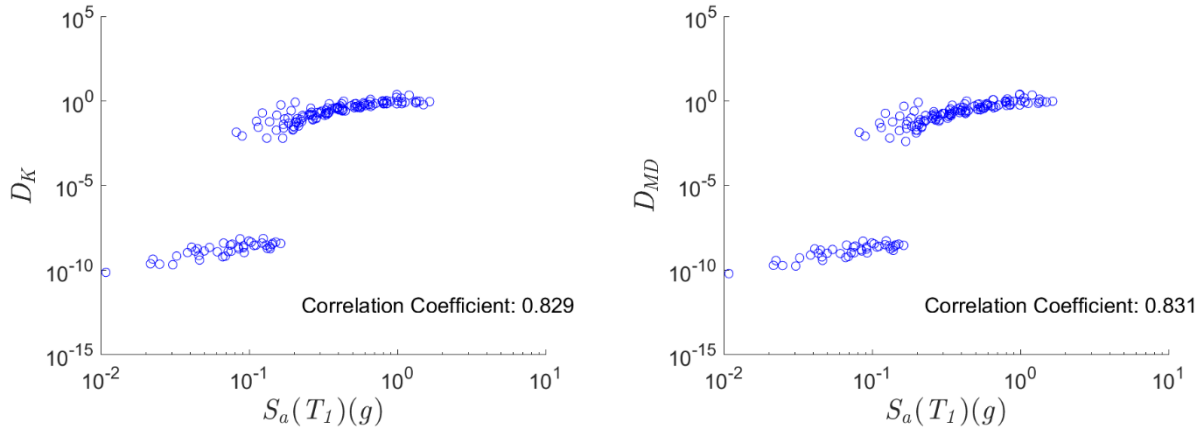

(c) (d)

Figure 4.3 Relationship between $S_a(T_1)$ and DM of (a) $MaxSDR$, (b) D_{PA}, (c) D_K and (d) D_{MD}

Figure 4.4 reveals the relationship between the energy-based damage measures and the drift-based damage measure. The horizontal axis is the energy-based damage indices and the vertical axis is the response in terms of the $MaxSDR$. The correlation coefficients between these four damage indices are also listed in Table 4-1. According to Table 4-1, the Park-Ang damage index D_{PA}, due to the participation of the deformation value in its calculation form, has the strongest correlation with the $MaxSDR$ among the energy-based damage indices. And there also appears a highly strong correlation between D_K and D_{MD} as expected because of the similarities in their formulas and calculations.

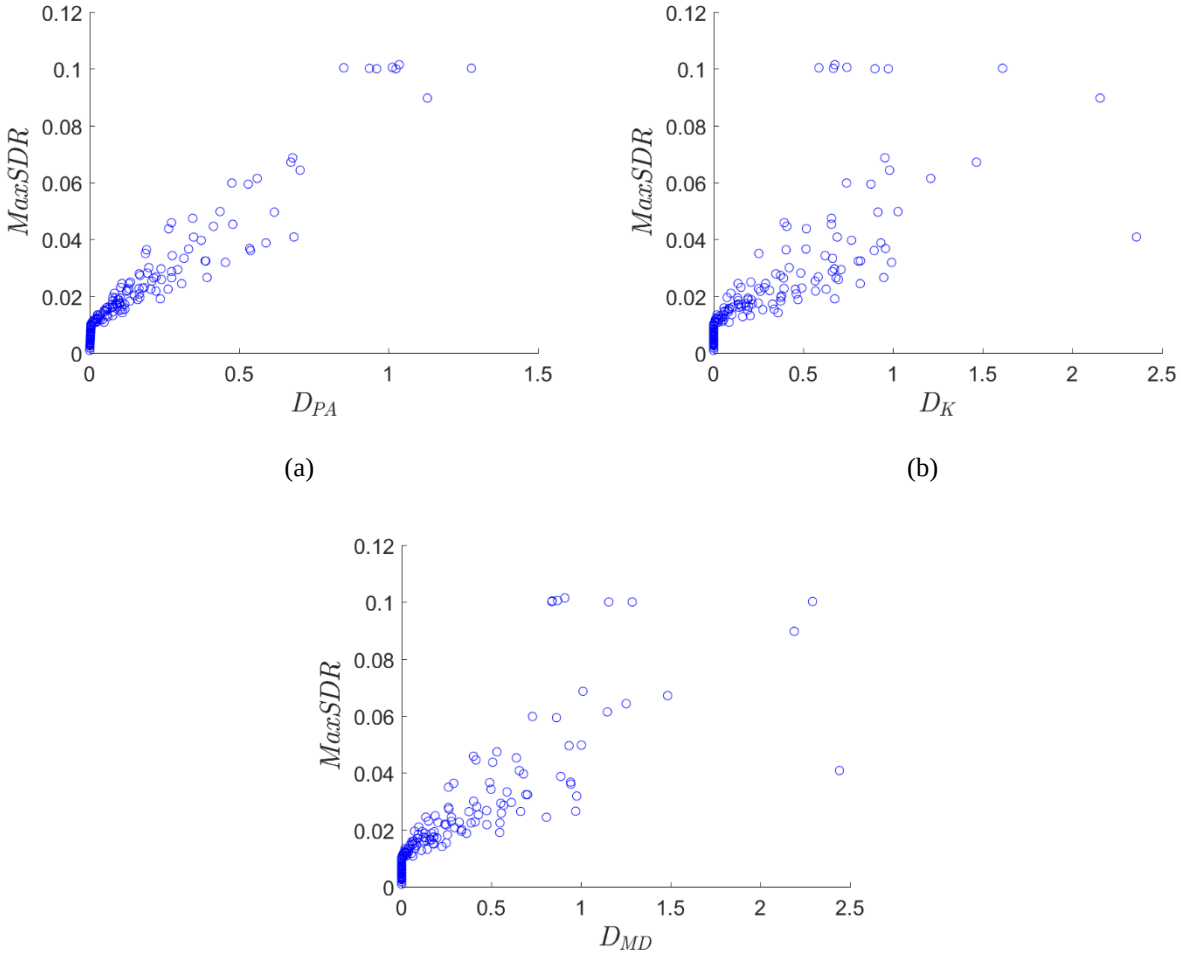

Figure 4.4 Correlation Relationship between the $MaxSDR$ and (a) D_{PA}, (b) D_K and (c) D_{MD}

Table 4-1 Correlation Coefficient between Damage Measures

Correlation Coefficient				
	$MaxSDR$	D_{PA}	D_K	D_{MD}
$MaxSDR$	1	0.9620	0.7554	0.8142
D_{PA}		1	0.8559	0.9105
D_K			1	0.9801
D_{MD}				1

For SDR, a value of 10% is a commonly-used value as the threshold of structural collapse and as such, in the numerical dynamic analyses, whenever a $MaxSDR$ of 10% is observed, the structure is assumed to have collapsed. For D_{MD}, the index exceeding 0.95 indicates collapse or total failure as recommended by Mehanny and Deierlein [6]. According to the plots in Figure 4.4, when the $MaxSDR$ goes beyond the collapse level of 10%, most of the energy-based damage indices would almost always appear at collapse or near-collapse level. Additionally, the energy-based indices also capture some points at collapse level when the story drift values are well below the 10% collapse threshold. As shown in Figure 4.4, in a number of analyses D_{MD} approaches 1, suggesting that collapse has happened in the structure whereas $MaxSDR$ is well below the 10% collapse threshold for the same analyses and still growing. Such trends are more or less observed for the remaining energy-based damage indices; suggesting that they are potentially more effective in characterizing structural collapse compared to $MaxSDR$.

4.3 Statistical Evaluation of Damage Measure

In order to evaluate the performance of alternative ground-motion intensity measures (IMs), Luco and Cornell [25] defined the concept of "efficiency" and "sufficiency" using the results of nonlinear structural dynamic analysis and linear regression analysis. Likewise, the concept of efficiency is applied to the damage measures (DMs) in this research. An efficient DM is the one that presents smaller variability or scatter when a certain IM level is given. Typically, the efficiency of an IM or a DM is measured using the standard deviation of the residual values from a linear regression quantitatively.

The $IM - DM$ relationships are displayed in Figure 4.5 and only the data points with $S_a(T_1) > 0.2g$ are selected in the plots. In the figure panels, a prediction model whose functional form is

shown in Equation 4.1 is fitted for all the DMs using the least squares method where the regression coefficients a and b are also indicated in the equations.

$$\log_{10} DM = a + b \log_{10} IM \tag{4.1}$$

The standard deviation of the regression residuals, $\sigma_{SD,residual}$, as a measure of efficiency, are listed in Table 4-2. The linear regression coefficients a and b are also included in Table 4-2. It is found that $MaxSDR$ is the most efficient DM among these four damage measures. It is, however, noteworthy that among the energy-based damage indices, the Mehanny-Deierlein damage index D_{MD} is the most efficient DM with a standard deviation that is not far from that of $MaxSDR$.

Table 4-2 Regression Coefficients of Damage Measures

Damage Measure (DM)		Regression Coefficients		
		a	b $(p-value)$	$\sigma_{SD,residual}$
Drift-based	$MaxSDR$	-1.290	0.852 (1.139e-24)	0.1453
	D_{PA}	-0.243	1.468 (3.576e-33)	0.4975
Energy-based	D_K	0.002	1.409 (5.482e-27)	0.2215
	D_{MD}	0.002	1.586 (1.186e-28)	0.2359

Additionally, comparison can be made on how strongly each of the damage measures are correlated with the IM level through performing statistical testing on the regression coefficient b. Based on the fitted linear curves, each DM presents different rates of increasement with IM as shown in Figure 4.5. The Mehanny-Deierlein damage index D_{MD} is linearly related to $S_a(T_1)$ through a coefficient of 1.586, which is notably higher than the $MaxSDR$'s coefficient of 0.852. The Park-Ang damage index D_{PA} and the Kratzig damage index D_K both have a relatively high

rate of increase between 1.4 to 1.5. The high rate of increase of D_{MD} with IM means that the this damage measure is more likely to identify the earthquake-induced damages developed in the studied building as it is being subjected to high-intensity ground motions compared to $MaxSDR$. This result is similar to Tesfariam and Goda's conclusion [8], which is drawn by analysis of a 15-story concrete building with shear walls.

Additionally, the $p-values$ of the regression coefficient b is also listed in Table 4-2. The reported $p-values$ correspond to the null hypothesis that there is no significant relationship between the damage measures and IM, i.e., the coefficient of the regression b is zero. A 5% $p-value$ is set to be the acceptable margin. If the $p-value$ is greater than 5%, then the null hypothesis that the Sa level and the DM are not correlated cannot be rejected. As illustrated in Table 4-2, although all the damage indicators have strong evidence to reject the null hypothesis with a very small $p-value$, the energy-based indices are more likely to be correlated with Sa level than the $MaxSDR$.

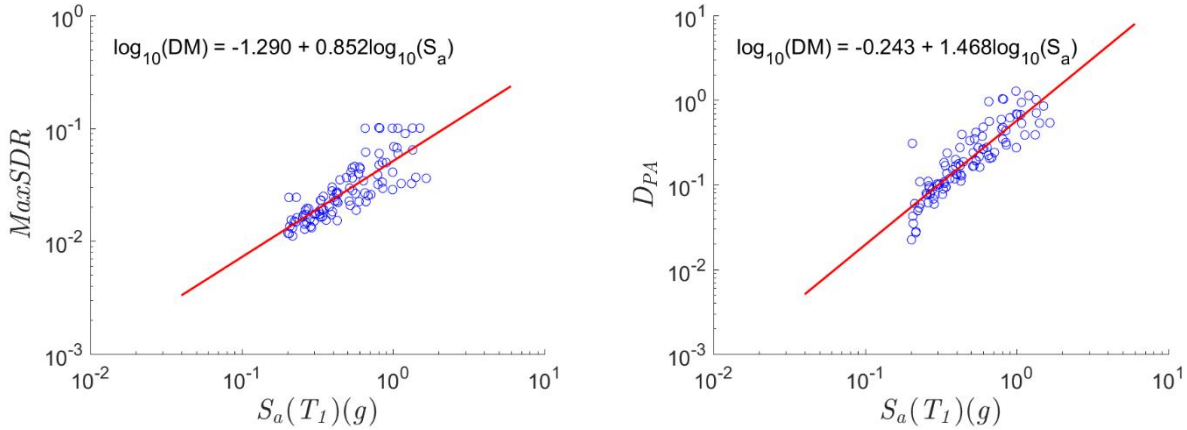

(a) (b)

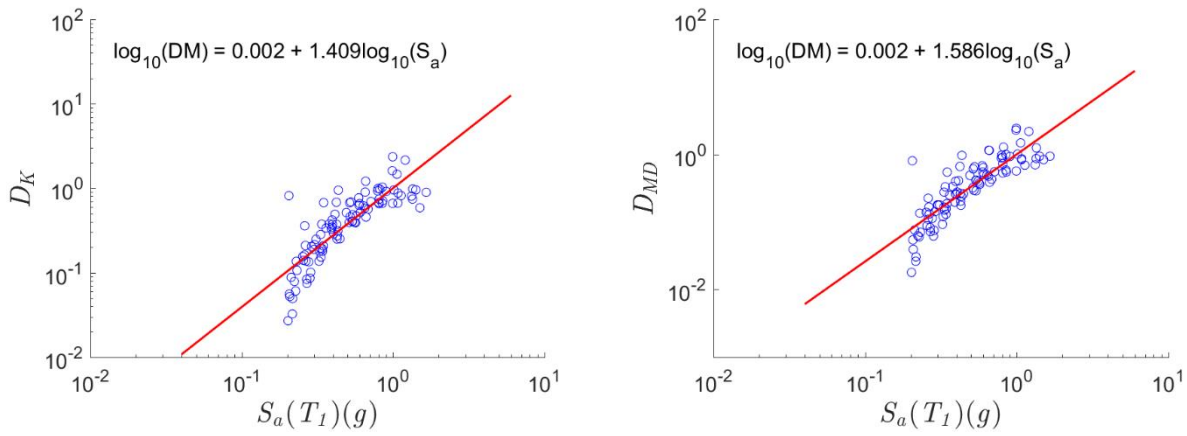

(c) (d)

Figure 4.5 Linear Regression of $S_a(T_1)$ and (a) $MaxSDR$, (b) D_{PA}, (c) D_K and (d) D_{MD} in log scale

Based on the calculated efficiency measures, the $MaxSDR$ is shown to be the most efficient damage measure and the D_{PA} is the least efficient DM. According to the comparison on the average increase rate, D_{MD} is the DM that is most capable of capturing the potential structural damage when the building experiences an earthquake with a high intensity. Hence, $MaxSDR$ and D_{MD} are used in seismic risk analysis as DM for the rest of this study.

Chapter 5 Seismic Risk Analysis under MS-AS Events

5.1 Methodology

The PBEE' methodology for computing the mean annual rate of exceeding a specified damage limit state is at the core of the structural seismic risk assessment and design. Mathematically, the mean annual rate of exceedance of a certain damage state, DS, which is denoted as $\lambda(DS)$, can be expressed as

$$\lambda(DS) = \iint G(DS|DM)|dG(DM|IM)||d\lambda(IM)| \tag{5.1}$$

In Equation 5.1, $d\lambda(IM)$ represents the mean annual frequency of exceeding a specific level of IM, which is typically obtained from PSHA. The term $G(DM|IM)$ denotes the probability of exceeding the DM level given the IM level of the ground motion. This value is calculated using the results of nonlinear dynamic analysis. In this research, this probability is computed from results of IDA illustrated in Chapter 4. Lastly, $G(LS|DM)$ denotes the probability of exceeding the pre-defined limit state given the value of the structural damage measure.

The PBEE methodology relies on the assumption that the structure remains in intact state prior to an earthquake event and the structure can always be repaired to its undamaged state before the occurrence of the next earthquake. This assumption is reasonable for mainshock-only situations since the time interval between two mainshock events is generally long enough for the repair measures to be completed. However, aftershock events normally have a high rate of occurrence in a relatively short time period after the mainshock happens. The structures that sustained a certain damage level in the mainshock event are usually not restored to their pre-mainshock state before the following aftershock event occur. As such, the uncertainty in the post-mainshock damage state

contributes to the uncertainty in predicting the structural damage state as the building is being subjected to the aftershock events. Thus, the traditional PBEE framework is not applicable in evaluating the structural seismic performance under the MS-AS sequences.

To theorize the time-dependent nature of aftershock events, Yeo and Cornell [26] extended the initial PBEE framework by the adoption of a Markov framework.

The probability of the structure shifting from the damage state under a seismic event to another state under the following event can be effectively accounted for by a Markov process approach. the Markov transition matrix, shown in Equation 5.2, quantify the transition probabilities between r pre-defined damage states under two consecutive seismic events.

$$\Pi = \begin{bmatrix} P_{11} & P_{12} & \cdots & P_{1r} \\ 0 & P_{22} & \cdots & P_{2r} \\ \vdots & \vdots & \ddots & \vdots \\ 0 & 0 & \cdots & 1 \end{bmatrix} \tag{5.2}$$

The term P_{ij} denotes the probability that the structure that has experienced damage state i after the previous earthquake transitions to damage state j when subjected to a following earthquake. In a short time interval case where the time is inadequate for building repair, the damage state can only become incrementally more severe, which is expressed in the upper triangular form of the Markov transition matrix. The diagonal elements of the Markov transition matrix indicate the likelihood that the damage condition of the structure remains unchanged after the following seismic event hence there is no damage state transition. The term P_{ij}, when $j > i$, in the transition matrix can be calculated using Equation 5.3. And the diagonal elements, defined as the probability of non-transition of damage states, can be easily calculated as the complement of the off-diagonal elements in each row.

$$P_{ij} = P_s\left(\int (P_{i,j}^{DS}[DS > ds_j|IM] - P_{i,j+1}^{DS}[DS > ds_{j+1}|IM])f_{IM}(im)dim\right) \tag{5.3}$$

The term P_s is the occurrence rate of the events that on the seismic source being considered that could potentially trigger the transition from damage state i to damage j. The term $P_{i,j}^{DS}[DS > ds_j|IM] - P_{i,j+1}^{DS}[DS > ds_{j+1}|IM]$ denotes the probability that the structure undergo the shift from damage state i to damage state j given the intensity measure (IM) of the following seismic event. The term $f_{IM}(im)$ is the probability density function (PDF) of the intensity measure at the site of the structure. This term is obtained from the PSHA which accounts for all the possible seismic events with different magnitudes and source-to-site distances. To model the effects of mainshock, a homogeneous Poisson process with the constant, time-independent rate of occurrence is used whereas the aftershock PSHA (APSHA) utilizes a nonhomogeneous Poisson process with a rate that accounts for the decaying rate of aftershock occurrence with time as shown in Equations 5.4 and 5.5. Given the time-dependent nature of aftershock seismic hazard, the seismic risk in the post-mainshock environment should also be expressed as a function of the elapsed time after the occurrence of mainshock.

$$P_S(N_{AS} = w) = \frac{(\mu_{AS})^w}{w!} e^{-\mu_{AS}} \tag{5.4}$$

$$\mu_{AS}(t_0, t_1) = \left(10^{a+b(M_m - M_0)} - 10^a\right) \frac{(t_1 + c)^{1-\rho} - (t_0 + c)^{1-\rho}}{1 - \rho} \tag{5.5}$$

The term $P_S(N_{AS} = w)$ denotes the probability that the number of aftershocks happening during the post-mainshock time interval is w. The term $P_S(N_{AS} = w)$ is calculated using the nonhomogeneous Poisson process and the μ_{AS} in this term is the mean rate of aftershock, which is time-dependent from APSHA. In Equation 5.5, (t_0, t_1) is the time interval where the occurrence rate of aftershocks is assessed. The terms M_m and M_0 are the moment magnitudes of causative mainshock and the following aftershocks. The generic parameters a, b, c and ρ are used to

generate the "generic model". In California, the aftershock events has the value of $a = -1.67$, $b = 0.91$, $c = 0.05$ and $\rho = 1.08$.

*U*nder the assumption that no more than a single time of aftershock can be generated in each predefined time interval, the Markov transition matrix that characterizes the limit state transition probabilities under aftershocks within the time interval (t_0, t_1) after the mainshock's occurrence can be calculated through Equation 5.6.

$$\Pi(t_0, t_1) = \begin{bmatrix} P_{11}(t_0, t_1) & P_{12}(t_0, t_1) & \cdots & P_{1r}(t_0, t_1) \\ 0 & P_{22}(t_0, t_1) & \cdots & P_{2r}(t_0, t_1) \\ \vdots & \vdots & \ddots & \vdots \\ 0 & 0 & \cdots & 1 \end{bmatrix} \tag{5.6}$$

Under the assumption of no more one aftershock in each time interval (t_0, t_1), At time step m after the occurrence of the mainshock, the probability that the structure is in damage state j given that it has already undergone damage state i under the mainshock is equal to the element on row i and column j of matrix P^m in Equation 5.7.

$$P^m = \prod_{i=1}^{m} \Pi(t_{i-1}, t_i) \tag{5.7}$$

The simplified Markov transition matrix discussed provides an efficient method of evaluating the seismic risk of the structure which has already experience a mainshock event and is now subjected to the following aftershocks. One might also be interested in performing seismic risk analysis in the pre-mainshock environment, where both the occurrence of the future mainshocks and their following aftershocks as well as the state of the structure once subjected to a future mainshock is unknown. The occurrence of mainshocks can be probabilistically modeled through conventional PSHA. This uncertainty in both the state of the structure once subjected to the mainshock as well the occurrence of the mainshock events can be incorporated into the Markov process by multiplying the aftershock limit state transition matrix in Equation 5.7 by a vector of

$P_{i,n}^{MS}$ values as shown in Equation 5.8. The summation in Equation 5.8 is on the all the seismic sources (N_s) that contribute to the seismic hazard at the site location of the building. The vector of $P_{i,n}^{MS}$ values represents the probability of the structure being in damage state $i, i = 1, \dots, r$ under mainshock ground motions and can be calculated using Equation 5.9.

$$P_{PreMS}^{m} = \sum_{n=1}^{N_S} \left(\left(P_{1,n}^{MS}, \dots, P_{r,n}^{MS}\right) \prod_{i=1}^{m} \Pi_n(t_{i-1}, t_i) \right) \tag{5.8}$$

$$P_{i,n}^{MS} = \int \left(P_{MS}^{DS}[DS > ds_i | IM] - P_{MS}^{DS}[DS > ds_{i+1} | IM]\right) df_{IM}^{n}(im) \tag{5.9}$$

The calculation of value of $P_{i,n}^{MS}$ is based on the results using the output data of nonlinear dynamic analysis under the MS-AS ground motion sequences. The entire nonlinear response history analysis is divided into two steps related to the mainshock analysis and the aftershock analysis, respectively. In the first step, the mainshock ground motions are scaled in order to generate a series of certain level of the damage measures. According to the results of comparison and evaluation in Chapter 4, the $MaxSDR$ and the D_{MD} are used as the damage measures in seismic risk analysis in this chapter. Three non-collapse different damage states based on different damage measures discussed and evaluated in Chapter 4 are targeted in this step. The range of those damage states are listed in Table 5-1. The intact state and the final damage defined as the global structural collapse state based on different damage measures showing the dynamic instability are also included in Table 5-1. The limit states for $MaxSDR$ are selected based on the SDR values reported in HAZUS technical manual for steel moment frame buildings, where SDR values of 0.4%, 0.8%, 2.0% and 5.33% are defined as the thresholds that mark Slight, Moderate, Extensive and Complete damage in the mid-rise steel moment frame buildings. The limit states for D_{MD} are suggested in Mehanny and Deierlein's report [6], where 0.25-0.3, 0.3-0.6 and 0.6-0.95 are suggested as the

ranges of limit states for immediate occupancy, life safety and near collapse, respectively, and 0.95 serves as the threshold of collapse. To obtain the structural damage at the target damage states, IDA analysis is utilized. Dynamic analysis is first performed under the mainshock ground motions that are scaled with a scale factor that would result in a $MaxSDR$ or D_{MD} level listed in Table 5-1. and then response history analysis is performed under the subsequent aftershock ground motions.

Table 5-1 Limit States Targeted in Risk Analysis

Damage Measure (DM)	Intact	Non-collapse Limit State			Collapse
MaxSDR	0.0%	0.4%	0.8%	2.0%	5.33%
D_{MD}	0.00	0.25	0.30	0.60	1.0

In the second step, the transition probability terms $P_{i,j}^{DS}[DS > ds_j|IM]$ in Equation 5.3 are obtained for the pre-defined damage states under the aftershock events. After the structure has experienced the mainshock event and sustained damage into damage state i, the pairing aftershock would be applied to the damaged building. The aftershocks are scaled to a series of spectral accelerations at the fundamental period of the structure ($S_a(T_1)$) as the IM value ranging from 0.2g to 2.8g. The output data of the response history analysis of the structure under the scaled MS-AS ground motion sequences are used to calculate the damage measure, through which the probability distribution and the fragility functions are calculated. Moreover, the probability of the limit states, combining with the time-dependent rate of occurrence of aftershock obtained from ASPHA would be used to compute the Markov transition matrix of Equation 5.6.

5.2 The Seismic Risk Analysis

Mainshock and aftershock seismic hazard analyses are performed for the site location of the studied building in Southern California, with a latitude and longitude of 33.996° and -118.169°. Mainshock hazard curve, which is calculated using conventional PSHA, as well as aftershock hazard curve obtained through APSHA are shown in Figure 5.1. The mean annual rate of occurrence $\lambda[S_a]$ is calculated with respect to $S_a(T_1)$, the spectral acceleration given the fundamental period (T_1) of the undamaged structure. For the traditional PSHA curve describing the mainshock seismic hazard, the contribution of 49 significant faults in total has been taken into consideration. In contrast, the APSHA curve for MS-AS events is calculated only considering the fault that has the highest contribution to the aftershock hazard at the building's location. APSHA is based on the assumption that a mainshock has already happened and now the seismic hazard due to the following aftershocks is being calculated. Since it is very unlikely for simultaneous ruptures to happen on multiple faults, the single fault that dominates the mainshock hazard is used in APSHA. Deaggregation of the site seismic hazard, performed using the tool provided by the USGS, shows that the Los Angeles section of the Puente Hills fault is the main source of mainshock seismic hazard. Therefore, the APSHA hazard curves in Figure 5.1 are obtained only for this fault. The APSHA hazard curves are calculated for a time window of one year starting immediately after the occurrence of the mainshock. The minimum magnitude is taken as 5 as events with smaller magnitudes are not likely to induce notable damage in modern code-conforming structures

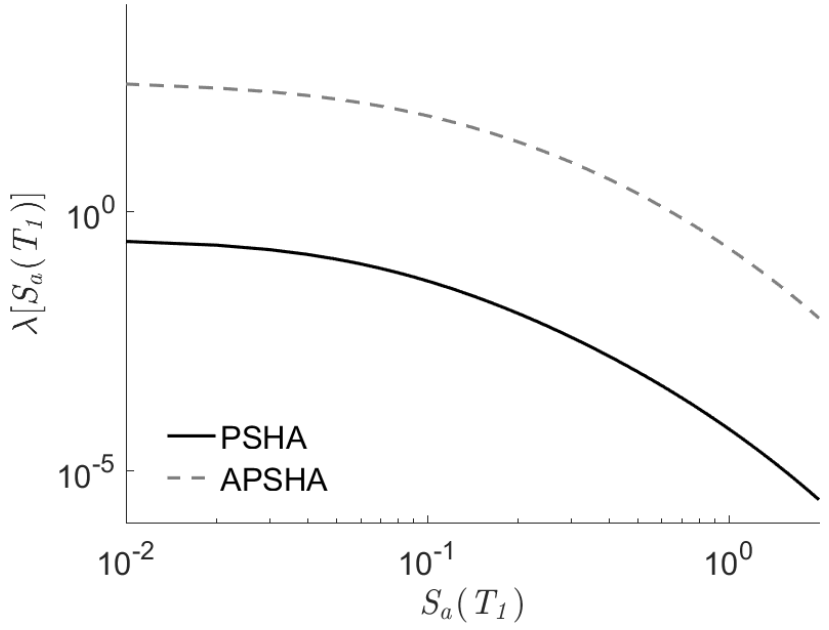

Figure 5.1 Mainshock and MS-AS Seismic Hazard Curves with $T_1 = 1.42\ sec$

Before the MS-AS seismic risk analysis is performed, the fragility curves of an intact structure under only-mainshock ground motions are calculated for the three non-collapse limit states along with the ultimate limit state of collapse described in Table 5-1. The $MaxSDR$ and the D_{MD} are used as the damage measure.

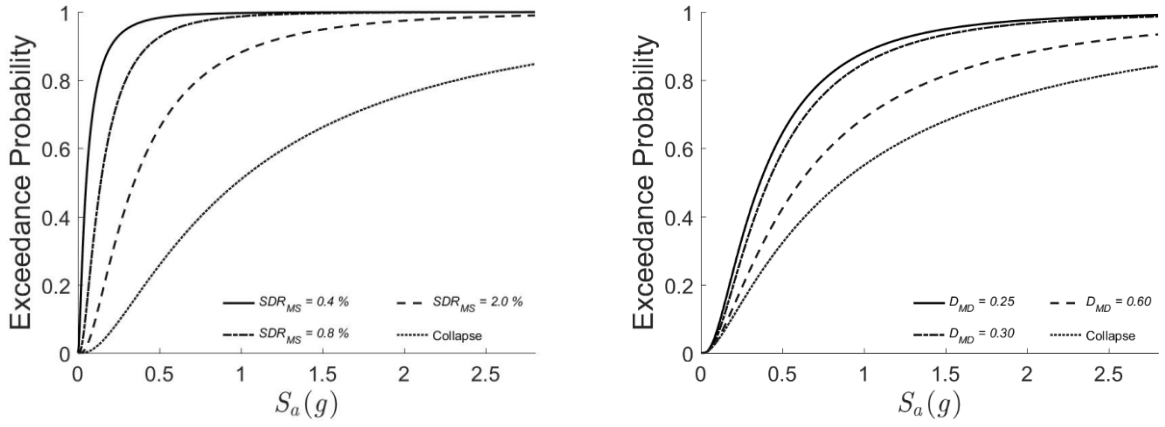

(a) (b)

Figure 5.2 Limit State Transition Fragility Curves for Mainshock Damage Level of (a) $MaxSDR$ and (b) D_{MD}

The limit state transition probabilities shown in Figure 5.3 and Figure 5.4 are obtained using Equation 5.3 assuming that a mainshock has happened on the Los Angeles section of the Puente Hills fault, the building is in one of the damage states defined in Section 5.1 and is now being subjected to the aftershocks that follow the mainshock.

The transitioning probability between different limit states due to the further damage in aftershock and the reduction in seismic capacity in mainshock events are calculated based on the results of MS-AS seismic risk analysis. With the increasing elapsed time after the occurrence of the mainshock event, the probability that the structure stays in the limit state that it has sustained under the mainshock drops continuously and the probability that the structure transitions into a severer damage state increases. A period of 7 days after the mainshock is selected to be the time window for the seismic risk estimation. As the time elapsed in the selected time window, the mean rate of occurrence of aftershock decreases continuously. Figure 5.3 shows the transitioning trend between the limit state with the $MaxSDR$ as DM. A rapid increase in probability of limit state transitioning is observed in all the curves in the beginning of the 7-day time period when the occurrence rate of aftershocks is at its peak stage while the probability that the structure remains in the damage state that it has experienced under the mainshock declines. In case that the structure remains in the intact state after experiencing the mainshock event, the possibility of building collapse would increase to about 1.0% and the probability that this building still remain intact will drop to 30% after 7 days using $MaxSDR$. If D_{MD} is used to measure the structural damage, the collapse probability in the end of 7-day period of the intact structure in the post-mainshock environment will stay at 10% level after a rapid increase in initial stage of the time window. It is also shown that for all corresponding post-mainshock structural damage level, the likelihood of

collapse after 7 days would be higher when D_{MD} is used as the damage measure compared to when $MaxSDR$ characterizes the collapse state.

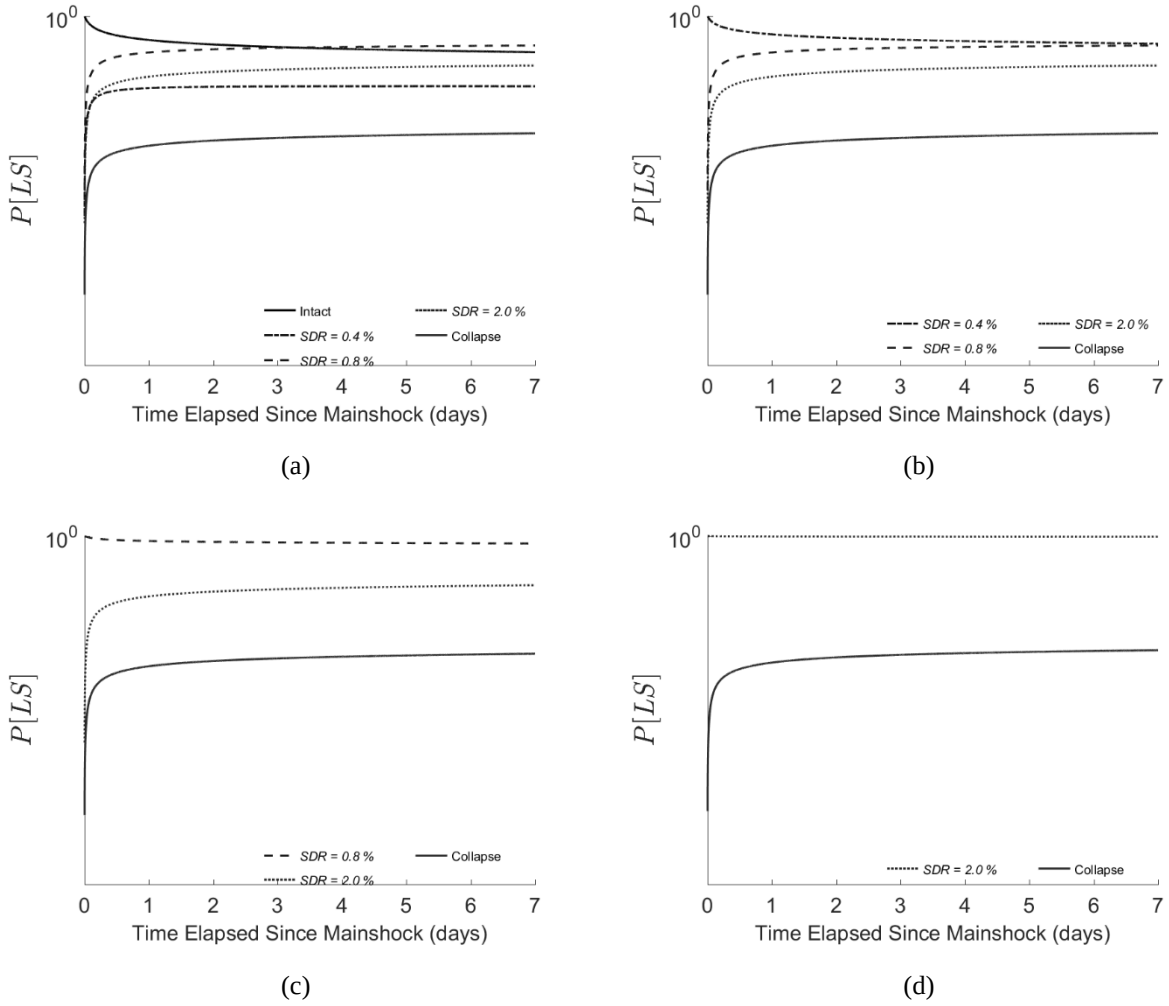

Figure 5.3 Limit State Transition Probabilities under Aftershock for (a) intact, (b) $MaxSDR = 0.4\%$, (c) $MaxSDR = 0.8\%$ and (d) $MaxSDR = 2.0\%$ for Mainshock Damage State

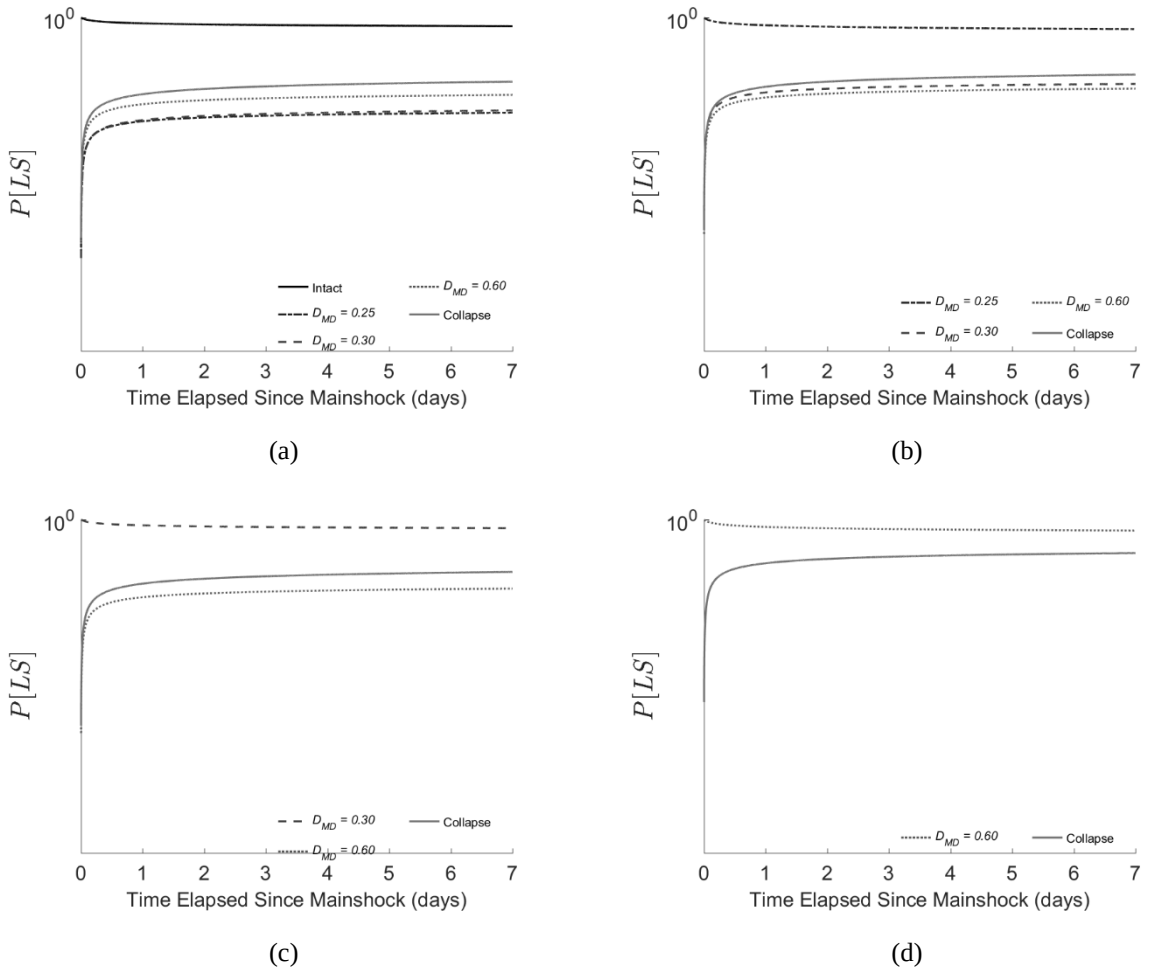

Figure 5.4 Limit State Transition Probabilities under Aftershock for (a) intact, (b) $D_{MD} = 0.25$, (c) $D_{MD} = 0.30$ and (d) $D_{MD} = 0.60$

Figure 5.5 compares the probability of transition between the selected limit states for the intact structure in the pre-mainshock situation assuming a lifespan of 50 years for the examined building. As shown, when the structure is subjected to MS-AS seismic sequences it would have a higher probability of experiencing any of the considered limit states compared to the case where the structure will only experience mainshocks.

Figure 5.6 compares the probability of collapse in the only-MS and MS-AS cases using different DMs. It displays that the collapse probability over the 50-year service of the building is

measured higher when D_{MD} is used to quantify building damage compared to when $MaxSDR$ is used to characterize collapse. This phenomenon indicates that, compared to $MaxSDR$, the energy-based damage measure is more capable of capturing structural damage developed under the MS-AS sequential seismic events.

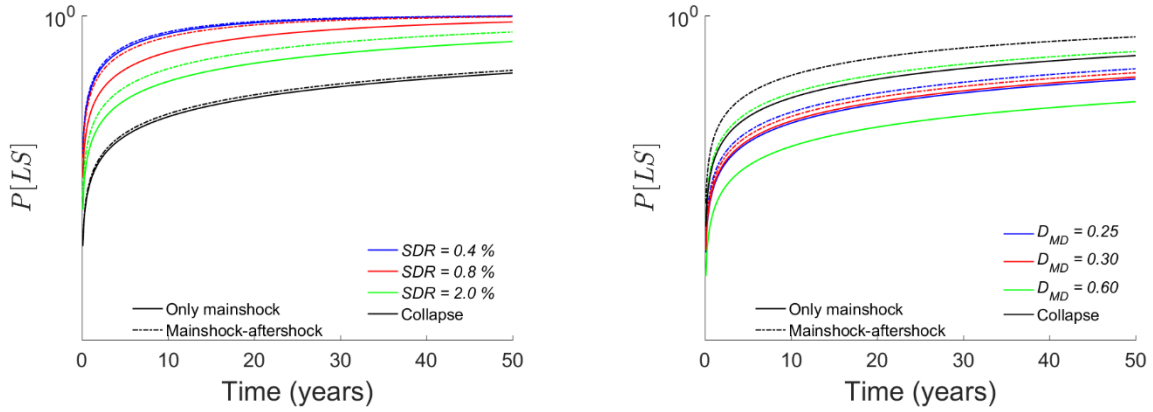

(a) (b)

Figure 5.5 Comparing Pre-mainshock MS-AS and Only Mainshock Limit State Transition Probability for (a) $MaxSDR$ and (b) D_{MD}

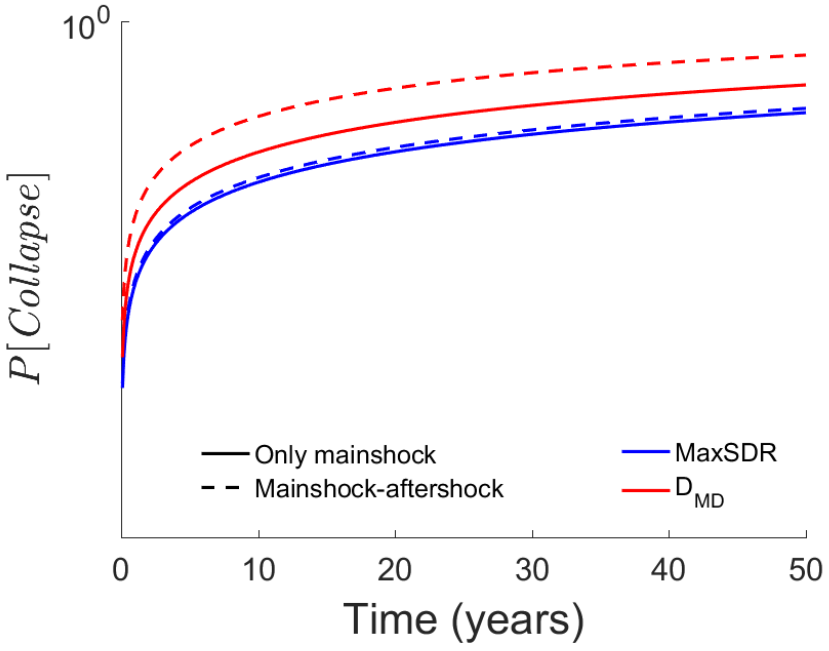

Figure 5.6 Probability of Collapse during Lifetime of Structures

It is worthy to note that in Figure 5.6, the probabilities of collapse at the end of the 50-year service life of the building under the MS-AS scenario are about 14% using $MaxSDR$ and 47% using D_{MD}, which are higher than what is usually expected for a code-conforming building. This is the result of the limited number of ground motion sequences used in the response history analyses. Since there are only 32 ground motion sequences selected, the lognormal distributions that characterize the building fragility curves have relatively high standard deviations. If, for example and for the sake of comparison, a value of 0.5 is manually assigned to the standard deviations of the fragility curves' distributions, the 50-year collapsed probability using the $MaxSDR$ would be 1.5% for only-mainshock case and 2.0% for MS-AS scenario, while the 50-year collapse probabilities using D_{MD} would be 2.2% for the only-mainshock case and 4.0% for the MS-AS case. Similar conclusion about how $MaxSDR$ and D_{MD} compare can still be made if a lower standard deviation is used for the collapse fragility curves.

Chapter 6 Conclusion

Characterizing seismic risk in structures can serve as a benchmark to evaluate a new design or identify the need to retrofit an existing building. A crucial factor in seismic risk analysis is the ability to capture the structural damage accurately when the building of interest is subjected to earthquake events with various intensities. Major seismic events are followed by a cluster of aftershocks that usually happen within a short period after the causative mainshock's occurrence. As such, structures are expected to experience higher levels of seismic risk in more realistic MS-AS scenarios compared to when only mainshocks are involved in risk analysis. Traditional damage measures, such as the maximum story drift ratio or peak floor acceleration, are most commonly used to characterize earthquake-induced structural damage in both practice and research. However, such damage measure sometimes fail to appropriately capture the damage developed in structural elements of a building after it is subjected to a seismic event. As a solution, some researchers have proposed a family of damage indices based on the introduces the amount of the hysteretic energy that structure absorbs during cyclic loading into the damage measure calculations. In this study, three energy-based damage indices, D_{PA}, D_K and D_{MD}, are compared with one of the traditional damage indicator, the maximum story drift ratio ($MaxSDR$).

The comparison and evaluation are based on the output data of dynamic analysis performed on the numerical model of a 4-story steel moment frame. The efficiency measure of DMs is used as the comparing criteria. The ability to capture the potential damage under the ground motion with lower intensity is also considered in the comparison and evaluation. It was observed that the $MaxSDR$ is the most efficient index with the lowest standard deviation of the residual values from the linear regression. The Mehanny-Deierlein damage index D_{MD} has the highest efficiency among

three energy-based indices. Thus, the $MaxSDR$ and the D_{MD} are utilized as DM in MS-AS risk analysis to make further comparison.

To further compare the abilities of $MaxSDR$ and D_{MD} damage measures in characterizing earthquake-induced damage, seismic risk analysis under sequential MS-AS ground motions are performed for the same steel frame building. Four limit states are targeted to compute the transitioning probability between different limit states using the Markov process framework. For both the only-mainshock and the MS-AS cases in the pre-mainshock environment, the D_{MD} shows a higher ability to characterize the collapse risk in the studied building, as it is marked by the higher collapse risk observed during the building's service life when D_{MD} is employed as the damage measure.

REFERENCE

[1] Cornell, C. Allin. "Engineering seismic risk analysis." *Bulletin of the seismological society of America* 58, no. 5 (1968): 1583-1606. Cornell, C. Allin. "Engineering seismic risk analysis." Bulletin of the seismological society of America 58.5 (1968): 1583-1606.

[2] Yeo, Gee Liek, and C. Allin Cornell. "A probabilistic framework for quantification of aftershock ground-motion hazard in California: Methodology and parametric study." *Earthquake Engineering & Structural Dynamics* 38, no. 1 (2009): 45-60.

[3] Gosain, Narendra K., Russell H. Brown, and J. O. Jersa. "Shear requirements for load reversals on RC members." *Journal of the Structural Division* 103, no. ASCE 13090 Proceeding (1977).

[4] Park, Young-Ji, Alfredo H-S. Ang, and Yi Kwei Wen. "Seismic damage analysis of reinforced concrete buildings." *Journal of Structural Engineering* 111, no. 4 (1985): 740-757.

[5] Krätzig, W. B., I. F. Meyer, and K. Meskouris. "Damage evolution in reinforced concrete members under cyclic loading." In *Structural Safety and Reliability*, pp. 795-804. ASCE, 1989.

[6] Mehanny, Sameh Samir Fahmy, and Gregory G. Deierlein. "Modeling and assessment of seismic performance of composite frames with reinforced concrete columns and steel beams." PhD diss., Stanford University, 1999.

[7] Estekanchi, H. E., K. Arjomandi, and A. Vafai. "Estimating structural damage of steel moment frames by endurance time method." *Journal of Constructional Steel Research* 64, no. 2 (2008): 145-155.

[8] Tesfamariam, Solomon, and Katsuichiro Goda. "Energy-Based Seismic Risk Evaluation of Tall Reinforced Concrete Building in Vancouver, BC, Canada, under Mw9 Megathrust Subduction Earthquakes and Aftershocks." *Frontiers in Built Environment* 3 (2017): 29.

[9] Lignos, D. G., H. Krawinkler, and A. S. Whittaker. "Prediction and validation of sidesway collapse of two scale models of a 4-story steel moment frame." *Earthquake Engineering & Structural Dynamics* 40, no. 7 (2011): 807-825.

[10] IBC, ICC. "International building code." *International Code Council, Inc.(formerly BOCA, ICBO and SBCCI)* 4051 (2006): 60478-5795.

[11] AISC, ANSI. "360-Specification for Structural Steel Buildings; American Institute of Steel Construction." (2005).

[12] Venture, SAC Joint, and Guidelines Development Committee. *Recommended seismic design criteria for new steel moment-frame buildings*. Washington, DC, USA: Federal Emergency Management Agency, 2000.

[13] Mazzoni, Silvia, Frank McKenna, Michael H. Scott, and Gregory L. Fenves. "The open system for earthquake engineering simulation (OpenSEES) user command-language manual." (2006).

[14] Ibarra, Luis F., Ricardo A. Medina, and Helmut Krawinkler. "Hysteretic models that incorporate strength and stiffness deterioration." *Earthquake engineering & structural dynamics*34, no. 12 (2005): 1489-1511.

[15] Shokrabadi, Mehrdad, Henry V. Burton, and Jonathan P. Stewart. "Impact of sequential ground motion pairing on MS-AS structural response and collapse performance assessment." *Journal of Structural Engineering*144, no. 10 (2018): 04018177.

[16] Goda, Katsuichiro. "Record selection for aftershock incremental dynamic analysis." *Earthquake Engineering & Structural Dynamics* 44, no. 7 (2015): 1157-1162.

[17] Ruiz-García, Jorge. "MS-AS ground motion features and their influence in building's seismic response." *Journal of Earthquake Engineering* 16, no. 5 (2012): 719-737.

[18] Abrahamson, Norman Alan, Walter Joseph Silva, and Ronnie Kamai. *Update of the AS08 ground-motion prediction equations based on the NGA-West2 data set*. Pacific Earthquake Engineering Research Center, 2013.

[19] Boore, David M., Jonathan P. Stewart, Emel Seyhan, and Gail M. Atkinson. "NGA-West2 equations for predicting PGA, PGV, and 5% damped PSA for shallow crustal earthquakes." *Earthquake Spectra* 30, no. 3 (2014): 1057-1085.

[20] Ancheta, Timothy D., Robert B. Darragh, Jonathan P. Stewart, Emel Seyhan, Walter J. Silva, Brian S-J. Chiou, Katie E. Wooddell et al. "NGA-West2 database." *Earthquake Spectra*30, no. 3 (2014): 989-1005.

[21] Park, Young-Ji, and Alfredo H-S. Ang. "Mechanistic seismic damage model for reinforced concrete." *Journal of structural engineering* 111, no. 4 (1985): 722-739.

[22] Cosenza, Edoardo, Gaetano Manfredi, and Roberto Ramasco. "The use of damage functionals in earthquake engineering: a comparison between different methods." *Earthquake engineering & structural dynamics* 22, no. 10 (1993): 855-868.

[23] Bozorgnia, Yousef, and Vitelmo V. Bertero. "Damage spectra: characteristics and applications to seismic risk reduction." Journal of Structural Engineering 129, no. 10 (2003): 1330-1340.

[24] Kemp, Alan R., and N. W. Dekker. "Available rotation capacity in steel and composite beams." *Structural engineer* 69 (1991): 88-97.

[25] Luco, Nicolas, and C. Allin Cornell. "Structure-specific scalar intensity measures for near-source and ordinary earthquake ground motions." *Earthquake Spectra* 23, no. 2 (2007): 357-392.

[26] Yeo, Gee Liek, and C. Allin Cornell. "Building life-cycle cost analysis due to mainshock and aftershock occurrences." *Structural Safety* 31, no. 5 (2009): 396-408.

[27] Shokrabadi, Mehrdad, and Henry V. Burton. "Risk-based assessment of aftershock and MS-AS seismic performance of reinforced concrete frames." *Structural Safety*73 (2018): 64-74.

[28] FEMA. "Hazus-MH 2.1 technical manual." *Multi-hazard loss estimation methodology, earthquake model* (2013).

[29] Baker, Jack W. "Efficient analytical fragility function fitting using dynamic structural analysis." *Earthquake Spectra* 31, no. 1 (2015): 579-599.